Semnan University

Journal of Heat and Mass Transfer Research

Journal homepage: https://jhmtr.semnan.ac.ir

ISSN: 2383-3068

Research Article

Bio-convective Magnetohydrodynamic flow of tangent hyperbolic nanofluid over a stretching surface with convective heat and slip conditions

Utpal Jyoti Das [a]*, Nayan Mani Majumdar [b]

[a] *Department of Mathematics, Gauhati University, Guwahati, 781014, India*

[b] *Department of Mathematics, Gauhati University, Guwahati, 781014, India*

ARTICLE INFO

Article history:

Received:

Revised:

Accepted:

Keywords:

Bioconvection;

Tangent hyperbolic fluid;

MHD;

Nanoparticles;

Microorganisms;

ABSTRACT

The current study investigates mixed convective flow of an unsteady MHD tangent hyperbolic nanofluid due to a stretching surface with motile micro-organisms via convective heat transfer and slip conditions. The flow analysis's governing equations were converted into a non-dimensional relation by using the proper alteration. The PDE model equations are computed for these transformed equations using MATLAB- bvp4c scheme. Skin friction, Sherwood number, Nusselt number, and the profiles of motile microorganisms are engineering-relevant quantities when compared to various physical variables. In comparison to recent literature, Skin friction is consistent for magnetic parameter, the results demonstrated a good consistency. Furthermore, an enhancement in the radiation and mixed convection parameter's magnitude enhances the velocity profile. Weissenberg number and magnetic field are used to study the reverse impact. The impact of thermal radiation parameter, Brownian movement, and thermophoretic effects are additional factors that frequently improve heat transfer. Through graphical and tabular explanations, the physical interpretation has been presented.

1. Introduction

A fascination brought on by the recent research of non-Newtonian fluids. Several researchers work in the mechanical, chemical, and technical fields in varying capacities. The easiest ways to come into contact with non-Newtonian fluids include polymeric relationships, atomic reactors, solvents, biomedical tumors, and many more. Non-Newtonian fluids might result in a non-linear correlation between shear rate and shear stress due to the complexity of their design and subsequent control using different type of model. Contrary to the Newtonian fluid, these fluids are so complicated that it is impossible to comprehend their rheological characteristics by a simple connection. Several researchers have studied the flow of non-Newtonian fluids such as Ali et at. [1], Alhadhrami et al. [2], Prameela et al. [3], Kumar et al. [4], Eswaramoorthi et al. [5], Mirzaee et al. [6], Das et al. [7], etc by considering different fluid model. The tangent hyperbolic fluid is one of the most well-known examples of a non-Newtonian fluid. The results show that such a structure predicts the thinning characteristic arising from shear with high accuracy. To be more precise, any substance that exhibits a pattern of shear-thinning characteristics may be examined using the tangent hyperbolic fluid

* **Corresponding author.**
E-mail address: mohammadi@gmail.com

Cite this article as:
Mohammadi, A., Mahdi-Nia, M., 2024. Title of article. *Journal of Heat and Mass Transfer Research*, 11(1), pp. 1402-1425.
https://doi.org/10.22075/JHMTR.2023.39315.2050

model. This fluid model is also known as the four-constant fluid model. In laboratories and industries, tangent hyperbolic fluids are often used. Some researches on tangent hyperbolic fluids are Ibrahim [8], Khan et al. [9], Bibi et al. [10], Salmi et al. [11], Faizan et al. [12], etc.

The fluid flow requires careful consideration of viscous dissipation when the fluid is moving at high speeds, raising its temperature. Typically, viscous dissipation is described as the variation of kinetic energy to internal energy, causing the fluid to become warmer, because of viscosity, which consists of kinetic energy generated by turbulent motion and average flow kinetic energy. Nowadays lots of research has been done on viscous dissipation, such as Gayatri et al. [13], Gopal et al. [14], Nalivela et al. [15], Li et al. [16], Das and Majumdar [17], Das et al. [18], etc.

The passage of an electric current through fluids, such as liquids and gases, can also cause joule heating. In this context, the term "joule heating" describes the procedure by which heat energy is produced by converting electrical energy inside the fluid medium. Joule heating in fluids is based on similar principles to that seen in solid conductors, with a few more factors to take into account. In order to move charges through a fluid, an electric current must overcome resistance. This resistance is largely affected by the fluid's electrical conductivity, which is controlled by elements including its composition and temperature. Heat is produced as a result of energy transfer caused by collisions between the moving electrons and the fluid's molecules. Ahmed et al. [19] did research showing the variations of joule heating on a Maxwell nanofluid flow passing through a slender surface. Some recent researches on joule heating are Waqas et al. [20], Naseem et al. [21], Chamkha et al. [22], etc.

The term "bioconvection" describes convective motions that take the form of patterns when swimming microorganism density move randomly in the form of cell colonies or certain cell types. Bio-convection is caused by microorganism density, which are migrating upward and are denser than water. Denser top walls created unbalanced suspensions when microorganisms sank to promote bio-convection. Several studies on bioconvection in nanofluids have been published recently. Researchers in this subject are interested in a number of applications of bioconvection employing microbes and nanoparticles in the fields of biosensors, biotechnology, mechanical energy, manufacturing, and bioinformatics. Microbes swim in the top zone because the structure is irregular and unstable. Because of the high density of stratification, the top area becomes imbalanced when the current microorganism swims on the higher surface. In marine habitats, such as river ponds, canyons, and seas, microbes lack constraints. Bioconvection has shown that microorganisms are swimming bacteria. The goal of bioconvection nano-liquids is to concentrate research on the impulsive configuration evolution and density stratification produced by simultaneously utilizing denser, self-driven microorganisms, nanoparticles, and drag forces. Working microorganisms may have organisms that exhibit gyrotaxis, gravitaxis, or oxytaxis. The inclusion of gyrotactic microorganisms in nano liquids enhances mass transference, microscale mixing, and nanofluid stability totally within micro volumes. Sajid et al. [23] show the influence of magnetohydrodynamics bioconvection tangent hyperbolic nanofluid on double-diffusive convection along motile microorganisms. Some other recent researches on bio-convection are Shi et al. [24], Waqas et al. ([25],[26]), Shah et al. [27], Hussain et al. [28], Rashid et al. [29], Kaswan et al. [30], Manai et al. [31], etc.

The aforementioned survey shows that no attempt has been made to look at bioconvection analysis on the magnetized flow of tangent hyperbolic nanofluid taking viscous dissipation along joule heating into consideration. Since viscous dissipation and joule heating are involved, our main goal is to carefully examine the numerical treatment of the bio-convection flow of tangent hyperbolic nanofluid. Additionally, the effects of velocity slips are offset. The MATLAB bvp4c tool is used to produce the numerical results. It is covered in detail how different parameters' graphical trends compare to subjective flow fields.

2. Mathematical formulation

To represent the flow of a non-Newtonian fluid, we must first understand its constitutive behaviour. In most non-Newtonian fluids, the constitutive relationship between the deviatoric stress tensor T and the applied strain rates E may be characterized by a time-independent scalar function $\mu = \mu\left(\dot{\gamma}\right)$ such that $T = 2\mu\left(\dot{\gamma}\right)E$. Here μ is the generalized velocity which depends on first principal invariant $\dot{\gamma} = \frac{1}{2}\sqrt{E:E}$ of the stress-strain rate tensor E. $\dot{\gamma}$ reduces to the shear rate in the basic shear flow scenario. There have been several functional forms proposed for $\mu\left(\dot{\gamma}\right)$, the most popular ones being the power-law model, the Carreau model, the Cross model, and the Herschel-Bulkley model.

In two-dimensional tangent hyperbolic nanofluid MHD, the flow of a motile microorganism over a stretching surface is conferred about. In this study, activation energy, nonlinear thermal radiation and convective boundary conditions were used, which can be used to enhance the rate of heat transfer. With a stream velocity of u_w, the flow would be perpendicular to the plane $y \geq 0$ (figure 1). The microorganism swims independently due to the direction of nanoparticles. This study uses the Cartesian coordinate in its mathematical formulation. The applied magnetic field is in the transverse direction of the plate.

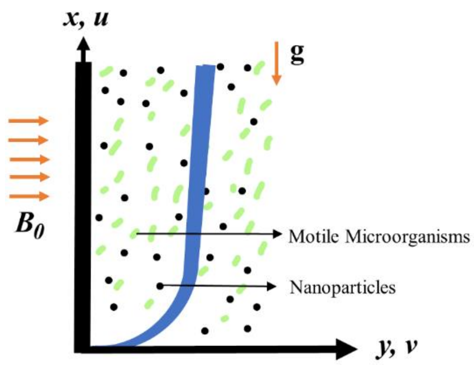

Figure 1: physical model

The constitutive equations for the model's flow are as follows (Ibrahim [8], Khan et al. [9]).

$$\frac{\partial u}{\partial x}+\frac{\partial v}{\partial y}=0 \tag{1}$$

$$u\frac{\partial u}{\partial x}+v\frac{\partial u}{\partial y}=\left(\begin{array}{l} \nu(1-n)\dfrac{\partial^2 u}{\partial y^2}-\dfrac{\sigma B_0^{\,2}}{\rho}u \\ +\sqrt{2}\nu n\Gamma\left(\dfrac{\partial u}{\partial y}\right)\left(\dfrac{\partial^2 u}{\partial y^2}\right) \\ +g\beta\left(1-C_\infty\right)\left(T-T_\infty\right) \\ -\dfrac{\gamma_1 g\left(\rho_m-\rho_f\right)\left(N-N_\infty\right)}{\rho_f} \\ -\dfrac{g\left(\rho_p-\rho_f\right)\left(C-C_\infty\right)}{\rho_f} \end{array}\right) \tag{2}$$

$$u\frac{\partial T}{\partial x}+v\frac{\partial T}{\partial y}-\tau\left[D_B\left(\frac{\partial C}{\partial y}\right)\left(\frac{\partial T}{\partial y}\right)+\frac{D_T}{T_\infty}\left(\frac{\partial T}{\partial y}\right)^2\right] = \left(\begin{array}{l} \left(\alpha_f\dfrac{\partial^2 T}{\partial y^2}+\dfrac{16\sigma T_\infty^{\,3}}{3k_f\left(\rho C_p\right)_f}\right)\dfrac{\partial^2 T}{\partial y^2}+\dfrac{\nu}{C_p}\left(\dfrac{\partial u}{\partial y}\right)^2 \\ +\dfrac{\sigma B_0^{\,2}}{\rho C_p}u^2 \end{array}\right) \tag{3}$$

$$u\frac{\partial C}{\partial x}+v\frac{\partial C}{\partial y}=D_B\frac{\partial^2 C}{\partial y^2}-K_0\left(C-C_\infty\right)+\left(\frac{D_T}{T_\infty}\right)\frac{\partial^2 T}{\partial y^2} \tag{4}$$

$$u\frac{\partial N}{\partial x}+v\frac{\partial N}{\partial y}=D_M\frac{\partial^2 N}{\partial y^2}-b\frac{W_c}{\left(C_w-C_\infty\right)}\frac{\partial}{\partial y}\left(N\frac{\partial C}{\partial y}\right) \tag{5}$$

The boundary restrictions are

$$\left.\begin{array}{l} u=u_w+U_{slip},\ v=0,\ D_B\dfrac{\partial C}{\partial y}+\dfrac{D_T}{T_\infty}\dfrac{\partial T}{\partial y}=0, \\ -k\dfrac{\partial T}{\partial y}=h_f\left(T_f-T\right),\ N=N_w \qquad at\ \ y=0 \\ u\to 0,\ v\to 0,\ C\to C_\infty,\ N\to N_\infty, \\ T\to T_\infty \qquad at\ \ y\to\infty \end{array}\right\} \tag{6}$$

The slip velocity U_{slip} is considered as (Wu [32])

$$U_{slip}=H\frac{\partial u}{\partial y}+S\frac{\partial^2 u}{\partial y^2} \tag{7}$$

Here H and S are constant.

Consider the transformations

$$\left.\begin{array}{l} \eta=y\sqrt{\dfrac{c}{\nu}},\ \ u=cxf'(\eta),\ \ \psi=\sqrt{c\nu}\,f(\eta), \\ v=-\sqrt{c\nu}\,f(\eta),\ \ \theta(\eta)=\dfrac{T-T_w}{T_w-T_\infty}, \\ \phi(\eta)=\dfrac{C-C_w}{C_w-C_\infty},\ \ \chi=\dfrac{N-N_w}{N_w-N_\infty} \end{array}\right\} \tag{8}$$

Using the transformations (8), the eqs. (2)-(5) becomes

$$\begin{array}{r} (1-n)f'''+nWi\,f''f'''-f'^2+ff''-Mf' \\ +\lambda(\theta-Nr\phi-Rb\chi)=0 \end{array} \tag{9}$$

$$\left(1+\frac{4}{3}Rd\right)\theta''+\Pr\left(\begin{array}{l} f\theta'+Nb\theta'\phi'+Nt\theta'^2 \\ +Ecf''^2+EcMf'^2 \end{array}\right)=0 \tag{10}$$

$$\phi''+\Pr Lef\phi'+\frac{Nt}{Nb}\theta''-\Pr Le\sigma^*\phi=0 \tag{11}$$

$$\chi''+Lbf\chi'-Pe\left(\chi'\phi'+\chi\phi''+\delta_1\phi''\right)=0 \tag{12}$$

The boundary restrictions are

$$\left.\begin{array}{l} f(\eta)=0,\ f'(\eta)=1+\alpha f''(\eta)+\beta f'''(\eta), \\ \theta'(0)=Bi\left(\theta(\eta)-1\right),\ Nb\theta'(\eta)+Nt\phi'(\eta)=0, \\ \chi(\eta)=1 \qquad at\ \ \eta=0 \\ f'\to 0,\ \theta\to 0,\ \phi\to 0,\ \chi\to 0 \qquad at\ \ \eta\to\infty \end{array}\right\} \tag{13}$$

Where

$$\left.\begin{array}{l} Wi=\dfrac{\sqrt{2c^3}\,x\Gamma}{\sqrt{\nu}},\ \lambda=\dfrac{g\beta(T_w-T_\infty)(1-C_\infty)}{c^2x},\\ Rb=\dfrac{\gamma_1\left(N_w-N_\infty\right)\left(\rho_m-\rho_f\right)}{\rho_f\beta(T_w-T_\infty)(1-C_\infty)},\ Lb=\dfrac{\nu}{D_M},\\ Nr=\dfrac{\left(\rho_p-\rho_f\right)\left(C_w-C_\infty\right)}{\rho_f\beta(T_w-T_\infty)(1-C_\infty)},Pe=\dfrac{bW_c}{D_M},\\ Nb=\dfrac{\tau D_B\left(C_w-C_\infty\right)}{\nu},\quad Nt=\dfrac{\tau D_T\left(T_w-T_\infty\right)}{\nu T_\infty},\\ M=\dfrac{\sigma B_0^2}{\rho c},\ Rd=\dfrac{4T_\infty^{\ 3}}{k_f\left(\rho C_p\right)_f},\ \Pr=\dfrac{\nu}{\alpha_f},\\ Le=\dfrac{\alpha_f}{D_B},\ Ec=\dfrac{c^2x^2}{\left(T_w-T_\infty\right)C_p},\ \sigma^*=\dfrac{K_0}{c}\\ \delta_1=\dfrac{N_\infty}{N_w-N_\infty}, \end{array}\right\} \quad (14)$$

Skin friction, Sherwood number, Nusselt number, and microorganism Sherwood number are as follows

$$\left.\begin{array}{l} C_f=\dfrac{2\tau_w}{\rho u_w^{\ 2}},\ Sh_x=\dfrac{xq_m}{D_M\left(C_w-C_\infty\right)},\\ Nu_x=\dfrac{xq_w}{\kappa\left(T_w-T_\infty\right)},\quad Nn_x=\dfrac{xq_n}{D_m\left(N_w-N_\infty\right)} \end{array}\right\} \quad (15)$$

Where τ_w is denoted for shear stress and heat flux is

$$q_w=-\kappa\left(\frac{\partial T}{\partial y}\right)_{y=0} \quad (16)$$

In the nondimensional form the equation (15) are as follows

$$\left.\begin{array}{l} C_f\sqrt{\mathrm{Re}_x}=\left((1-n)f''(0)+\dfrac{n}{2}Wif''(0)^2\right),\\ \dfrac{Sh_x}{\sqrt{\mathrm{Re}_x}}=-\phi'(0),\\ \dfrac{Nu_x}{\sqrt{\mathrm{Re}_x}}=-\left(1+\dfrac{4}{3}Rd\right)\theta'(0),\\ \dfrac{Nn_x}{\sqrt{\mathrm{Re}_x}}=-\chi'(0), \end{array}\right\} \quad (17)$$

3. Solution methodology

The set of the highly nonlinear, non-dimensional equation (9–12) subjected to boundary restriction (13) is a two-point boundary-value problem. A well-known tool called bvp4c is used under MATLAB for the solution of the equations.

Therefore, to implement bvp4c, paired non-dimensional differential equations with boundary restrictions must be reduced into a first-order simultaneous equations system. Let

$$\left.\begin{array}{l} f=\Gamma_1,\quad f'=\Gamma_2,\quad f''=\Gamma_3,\quad f'''=\Gamma_3',\\ \theta=\Gamma_4,\quad \theta'=\Gamma_5,\quad \theta''=\Gamma_5',\\ \phi=\Gamma_6,\quad \phi'=\Gamma_7,\quad \phi''=\Gamma_7',\\ \chi=\Gamma_8,\quad \chi'=\Gamma_9,\quad \chi''=\Gamma_9',\\ \Gamma_3'=\dfrac{\begin{pmatrix}\Gamma_2^{\ 2}+M\Gamma_2-\Gamma_1\Gamma_3\\ -\lambda\left(\Gamma_4-Nr\Gamma_6-Rb\Gamma_8\right)\end{pmatrix}}{1-n+nWi\Gamma_3},\\ \Gamma_5'=\dfrac{-\Pr\begin{pmatrix}\Gamma_1\Gamma_5+Nb\Gamma_5\Gamma_7+Nt\Gamma_5^{\ 2}\\ +Ec\Gamma_3^{\ 2}+Ecm\Gamma_2^{\ 2}\end{pmatrix}}{\left(1+\dfrac{4}{3}Rd\right)},\\ \Gamma_7'=-\dfrac{Nt}{Nb}\Gamma_5'-\Pr Le\Gamma_1\Gamma_7+\Pr Le\sigma^*\Gamma_6,\\ \Gamma_9'=Pe\left[\Gamma_7\Gamma_9+\left(\Gamma_8+\delta_1\right)\Gamma_7'\right]-Lb\Gamma_1\Gamma_9 \end{array}\right\} \quad (18)$$

with conditions

$$\left.\begin{array}{l} \Gamma_1=1+\alpha\Gamma_2+\beta\Gamma_3,\ \Gamma_5=Bi\left(\Gamma_4-1\right),\\ Nb\Gamma_5+Nt\Gamma_7=0,\ \Gamma_8=1\quad at\quad \eta=0\\ \Gamma_2\to 0,\ \Gamma_4\to 0,\ \Gamma_6\to 0,\\ \Gamma_8\to 0\qquad\qquad at\ \eta\to\infty \end{array}\right\} \quad (19)$$

4. Results and discussion

Boundary conditions (13) are used to solve equations (9–12) using MATLAB's bvp4c solver, and the results are graphically displayed for the velocity profile, temperature, concentration, and motile microorganism density profile. Numerical solution arrived at converged on the boundary restrictions without any errors or warnings. This indicates that the established tolerance limit is supported by the numerical solution.

Unless otherwise specified, the emerging parameter values are taken as $n=0.3,\ Wi=0.3,\ Rd=0.8,\ M=0.2,\ \Pr=0.71, \alpha=1,$ $Nb=0.5,\ Rb=0.1,\ Nt=0.5,\ Le=5,\ Bi=2,\ \lambda=0.1,$ $Nr=0.1,\ Ec=0.1,\ \sigma^*=0.1,\ Pe=1, \delta_1=0.1,\ Lb=0.2,$ $\beta=-1$

Figure 2-7 shows the effects of *M, Wi, n, Rd, Pr* and λ. Figure 2 shows *M* decreases the velocity. It is obvious that for bigger values of *M*, the velocity will decline due to the increase in the Lorentz force. Figure 3 shows Wi decreases the velocity. Wi is the ratio of the fluid's relaxation time to a certain process time, when the Weissenberg number grows, the fluid's relaxation time also increases. This provides resistance for the fluid particles, which lowers the fluid's velocity. Figure 4 shows n decreases the velocity. It becomes evident when the greater value of n depreciates in the fluid velocity. This property affects the fluid's viscosity, physically. Shear thinning is exhibited by the fluid for small values of n, shear thickening is seen for greater values of n, and Newtonian behavior is exhibited when n = 1. A weaker velocity field results when n is greater than one because the fluid's velocity declines. Figure 5 shows Rd increases the velocity. By improving the thermal radiation parameter, the fluid's thermal conditions are significantly improved. This results in greater fluid volume in the boundary layer as a result of the buoyancy effect, which raises the fluid's velocity. Figure 6 shows Pr reduces fluid velocity whereas Figure 7 shows that λ increases fluid velocity.

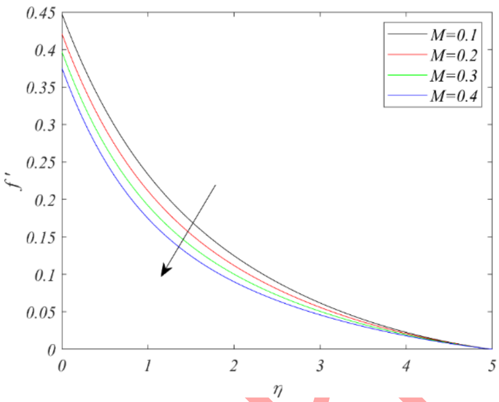

Figure 2: Variations of M on velocity

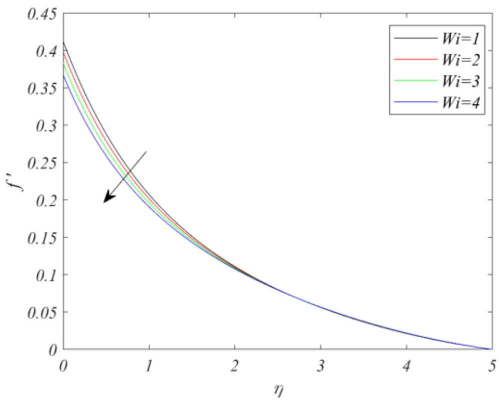

Figure 3: Variations of Wi on velocity

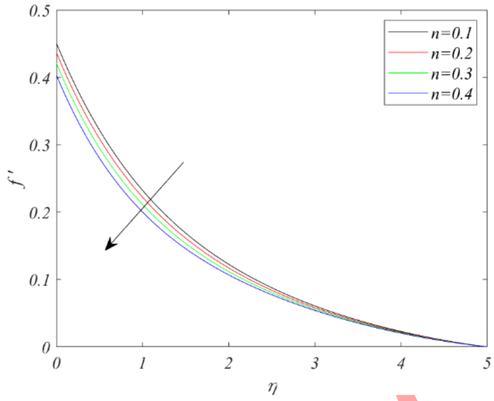

Figure 4: Variations of n on velocity

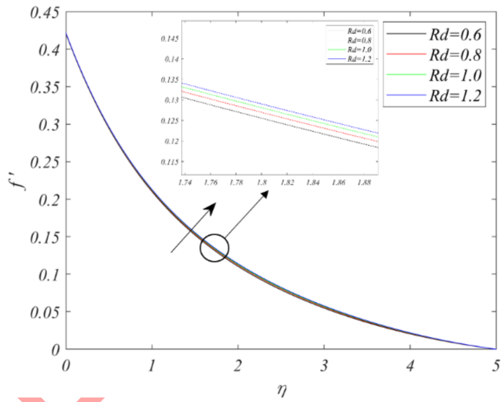

Figure 5: Variations of Rd on velocity

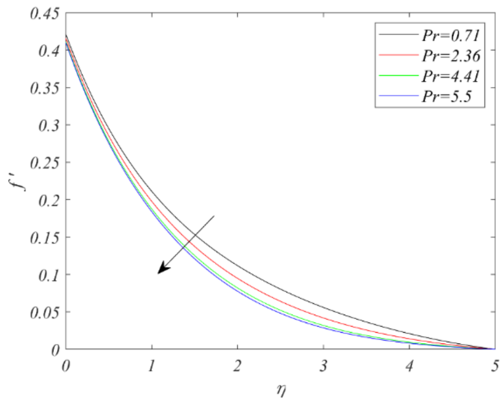

Figure 6: Variations of Pr on velocity

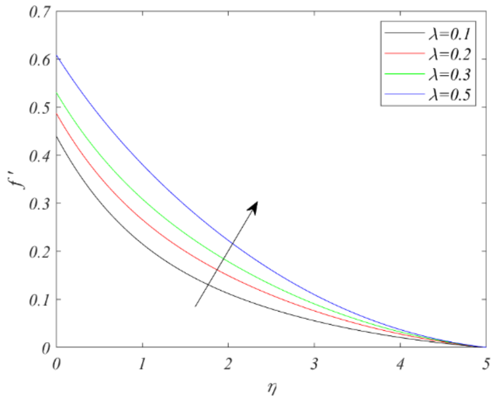

Figure 7: Variations of λ on velocity

Figure 8-14 displays how temperature is impacted by *M, Wi, n, Rd, Pr, Nr,* and *Nt*. The temperature is rising in Figure 8 caused by *M*. As the magnetic parameter increases, the boundary layer's temperature rises but the magnitude of its velocity profiles decreases. The thermal boundary layer thickness has increased, as seen in Figure 9, leading to a rise in temperature. Figure 10 demonstrates that fluid temperature rises with *n*, since it directly influences the energy equation, it is obvious that the power law index has an impact on the temperature distribution. On the other hand, the power law index has a negligible and small impact on the temperature distribution because of its indirect influence on the concentration field. The temperature is raised by *Rd*, as seen in Figure 11. Heat is transported from the heated wall to the fluid due to the fluid's ability to absorb its own radiation. Figure 12 demonstrates how *Pr* lowers the temperature. As the Prandtl number increases, the thermal boundary layer thickness decreases. *Pr* is used to describe the relationship between momentum and thermal diffusivity. *Pr* controls the relative thickness of the momentum and thermal boundary layers. Figure 13 depicts a temperature increase caused by *Nr*. *Nt* causes the temperature to rise, as shown in Figure 14. This is because particles near hot surfaces produce a thermophoretic force that promotes particle breakdown outside of the fluid regime (on the cylinder), increasing temperature and concentration boundary layer thicknesses.

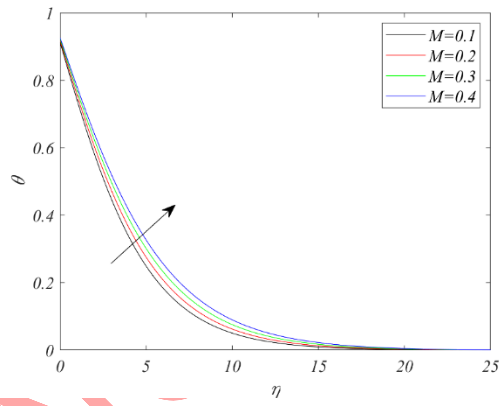

Figure 8: Variations of *M* on temperature

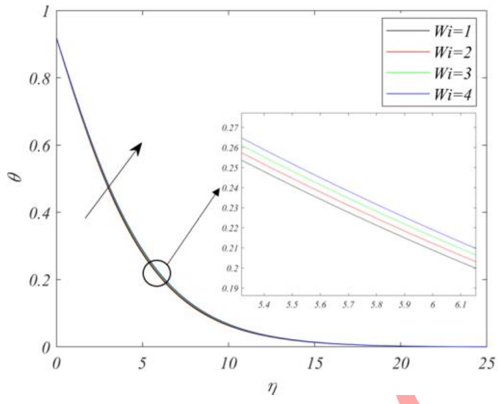

Figure 9: Variations of *Wi* on temperature

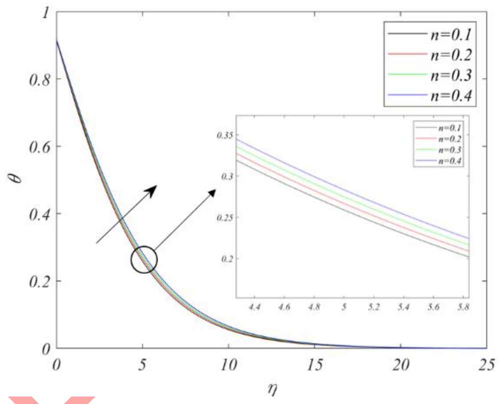

Figure 10: Variations of *n* on temperature profile

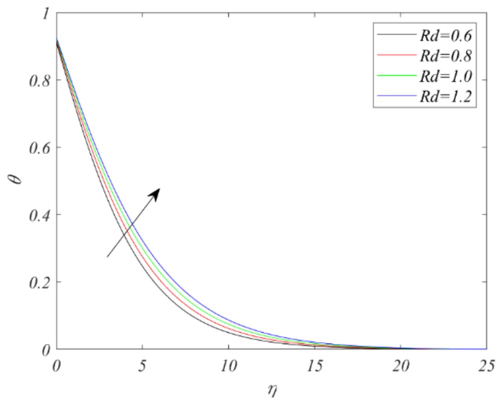

Figure 11: Variations of *Rd* on temperature

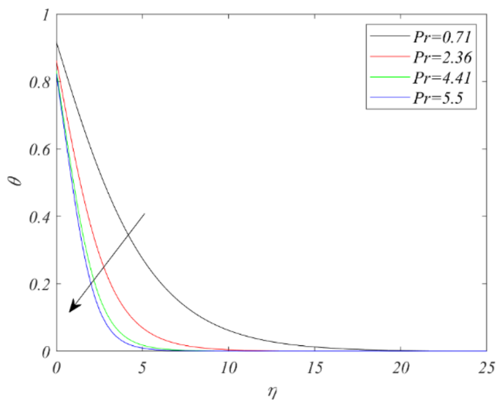

Figure 12: Variations of *Pr* on temperature

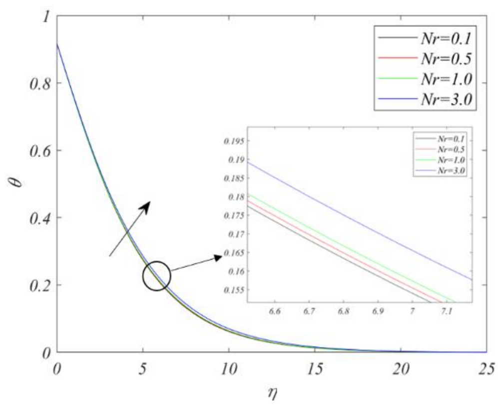

Figure 13: Variations of *Nr* on temperature

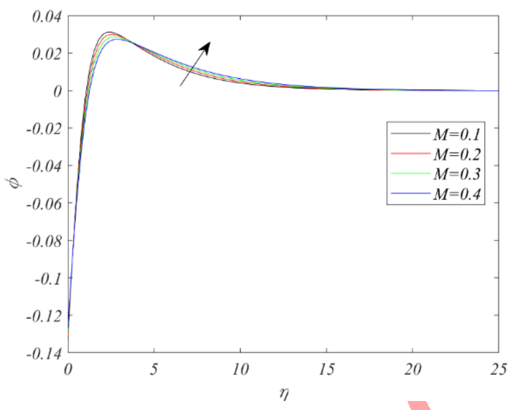

Figure 15: Variations of *M* on concentration

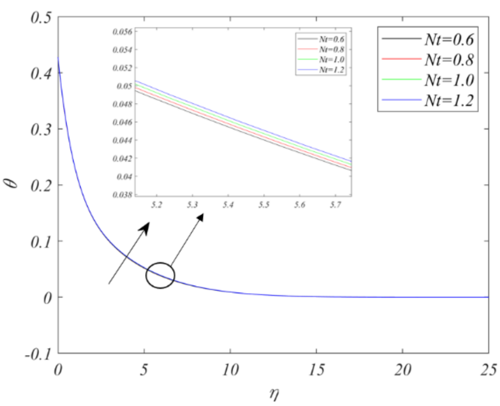

Figure 14: Variations of *Nt* on temperature

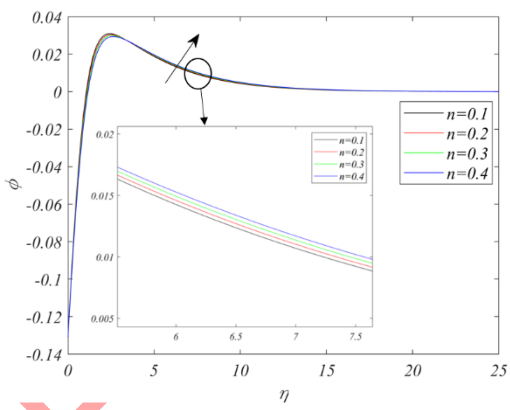

Figure 16: Variations of *n* on concentration

Figure 15-20 shows the effects of *M, n, Pr, Le, Nb* and *Nt* on the field of concentration. Figure 15 shows that *M* increases the concentration field. Figure 16 shows that *n* increases the concentration field, an enhancement in value of *n*, the fluid becomes more viscous, resulting concentration field improved. Figure 17 shows that *Pr* decreases the concentration field. Figure 18 shows that *Le* decreases the concentration field. In boundary layer, Lewis number identifies the proportion of thermal diffusion rate to species diffusion rate. According to the definition, *Le* is the ratio of the Schmidt to the Prandtl numbers; as a result, Heat will diffuse more quickly than species when *Le* is greater than 1.0, and will diffuse at the identical rate when *Le = 1*. When Lewis number is raised, the concentration profiles become steeper and the species boundary layer thins. Figure 19 shows that *Nb* decreases the concentration field due to Brownian motion's ability to warm the boundary layer, which causes the particles to leave the fluid regime. Figure 20 shows that *Nt* increases the concentration field of the fluid.

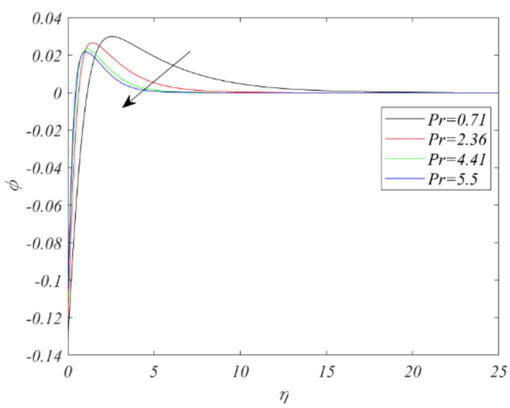

Figure 17: Variations of *Pr* on concentration

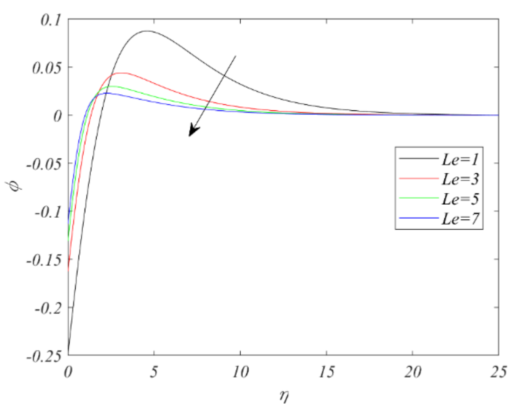

Figure 18: Variations of *Le* on concentration

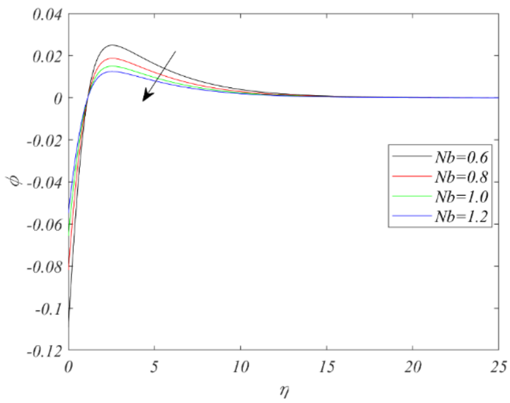

Figure 19: Variations of *Nb* on concentration

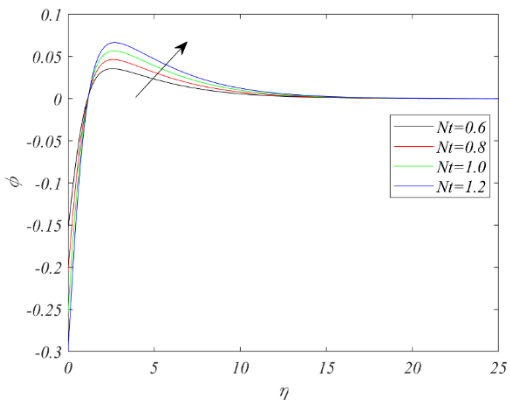

Figure 20: Variations of *Nt* on concentration

Figures 21-25 show the effects of *n, Pe, Lb, Nb* and *Le* on motile microorganism density χ. Figure 21 shows that n increases the motile microorganism density χ. An increase in *n*, the fluid turns more viscous which improves motile microorganism density. Figure 22 and figure 23 shows that *Pe* and *Lb* decrease the motile microorganism density χ. A gradual decline in the motile microorganism density of fluid is observed because the diffusivity of the microorganism decays with increasing Lewis number *Lb*. The thickness of microorganism density decreased in accordance with rising Peclet number *Pe* values. With an improvement in Peclet number, the cell swimming speed accelerates. As the number of bio-convection Peclets rises, motile microorganism density degrades. It is seen that the motile microorganisms' distribution's diffusivity of the nanofluid decreases in both cases. Figure 24 and figure 25 show that *Nb* and *Le* decrease the motile microorganism density χ.

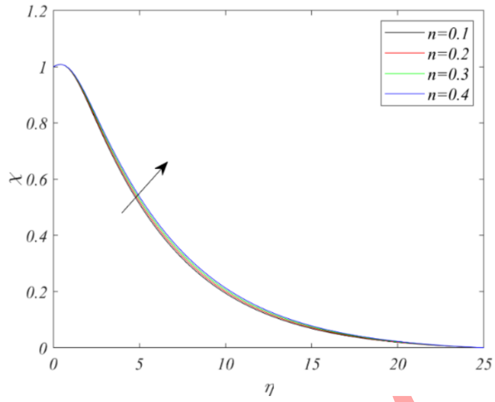

Figure 21: Variations of *n* on motile microorganism density

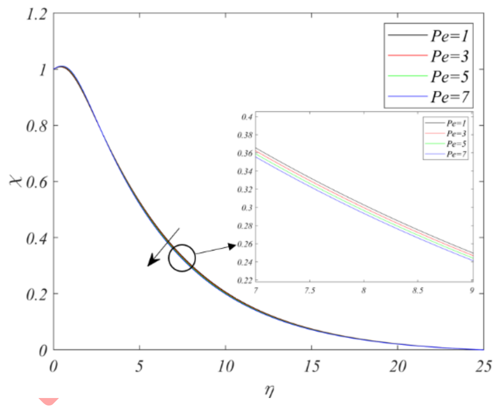

Figure 22: Variations of *Pe* on motile microorganism density

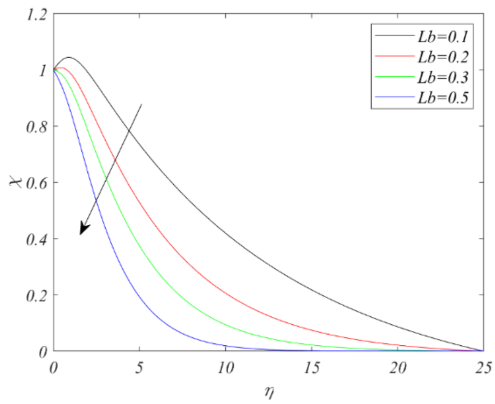

Figure 23: Variations of *Lb* on motile microorganism density

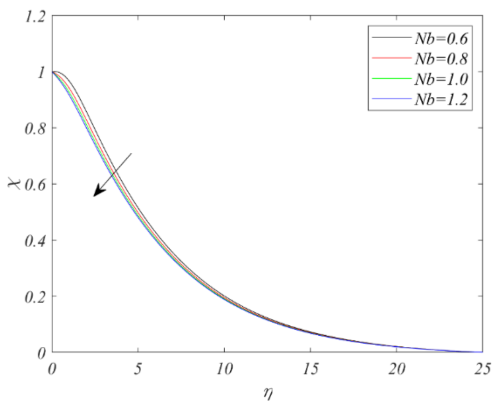

Figure 24: Variations of *Nb* on motile microorganism density

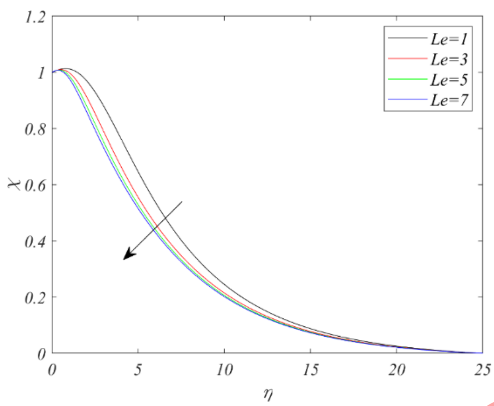

Figure 25: Variations of *Le* on motile microorganism density

Table 1 shows that *M, Nr, Rb* increases the Skin friction values whereas λ shows opposite pattern. Table 2 shows that *M, Wi, n, Rd, Nt* reduces Nusselt number values whereas Pr shows opposite pattern. Table 3 shows that microorganism density is boosted by increasing the *Lb* values and declining the *Pe* values.

Table 1: Variations of $-f''(0)$ for distinct parameters.

M	Nr	Rb	λ	$-f''(0)$
0.2	0.1	0.1	0.1	0.3098
0.3	0.1	0.1	0.1	0.3116
0.4	0.1	0.1	0.1	0.3127
0.2	0.1	0.1	0.1	0.3098
0.2	0.2	0.1	0.1	0.3101
0.2	0.3	0.1	0.1	0.3105
0.2	0.1	0.1	0.1	0.3098
0.2	0.1	0.2	0.1	0.3132
0.2	0.1	0.3	0.1	0.3167
0.2	0.1	0.1	0.1	0.3098
0.2	0.1	0.1	0.2	0.2952
0.2	0.1	0.1	0.3	0.2846

Table 2: Variations of $-\theta'(0)$ for different parameters.

M	Wi	n	Rd	Nt	Pr	$-\theta'(0)$
0.2	0.3	0.3	0.8	0.5	0.71	0.2222
0.3	0.3	0.3	0.8	0.5	0.71	0.2180
0.4	0.3	0.3	0.8	0.5	0.71	0.2144
0.2	0.3	0.3	0.8	0.5	0.71	0.2222
0.2	0.4	0.3	0.8	0.5	0.71	0.2220
0.2	0.5	0.3	0.8	0.5	0.71	0.2219
0.2	0.3	0.3	0.8	0.5	0.71	0.2222
0.2	0.3	0.4	0.8	0.5	0.71	0.2199
0.2	0.3	0.5	0.8	0.5	0.71	0.2175
0.2	0.3	0.3	0.8	0.5	0.71	0.2222
0.2	0.3	0.3	0.9	0.5	0.71	0.2198
0.2	0.3	0.3	1.0	0.5	0.71	0.2177
0.2	0.3	0.3	0.8	0.5	0.71	0.2222
0.2	0.3	0.3	0.8	0.7	0.71	0.2186
0.2	0.3	0.3	0.8	0.9	0.71	0.2150
0.2	0.3	0.3	0.8	0.5	0.71	0.2222
0.2	0.3	0.3	0.8	0.5	0.81	0.2272
0.2	0.3	0.3	0.8	0.5	0.95	0.2342

Table 3: Variations of $-\chi'(0)$ for different parameters.

Pe	Lb	$-\chi'(0)$
1	0.2	0.0361
2	0.2	0.0184
3	0.2	0.0045
1	0.2	0.0361
1	0.3	0.0557
1	0.4	0.0759

5. Validity and comparisons

To prove the validity of the current study, the findings are contrasted with previously published results provided by Ibrahim [8], Khan et al. [9] and Waqas et al. [26].

Table 4 demonstrates the present results are identical with the results of Ibrahim [8], Khan et al. [9] and Waqas et al. [26], and are found in good agreement.

M	Khan et al. [9]	Waqas et al. [26]	Ibrahim [8]	Present result
0	-1.0000	-1.0000	-1.0000	-1.0000
0.25	---	-1.1180	-1.1180	-1.1180
1.0	-1.4139	-1.4142	-1.4142	-1.4142
5.0	-2.4499	-2.4495	-2.4495	-2.4495
10	-3.3170	-3.3166	-3.3166	-3.3166
100	-10.0503	-10.0499	-10.0499	-10.0499

6. Conclusions

The topic of the ongoing study is the tangent hyperbolic nanofluid flow caused by moving microorganisms and second-order velocity slip. A study is done on how Brownian motion and thermophoresis affect fluid.

Using the MATLAB- bvp4c scheme, the remodeled ODEs system is numerically handled. The following outcome has been found

- *Rd* and λ enhanced the fluid velocity while *M, Wi* and *Pr* show opposite patterns.
- *M, Wi, n, Rd, Nr* and *Nt* enhanced the temperature profile while *Pr* shows the opposite pattern.
- *M, n* and *Nt* to grow Concentration profile whereas it shows the opposite pattern for *Pr, Le* and *Nb*.
- *Pe, Lb, Nb* and *Le* decline the motile microorganism density whereas n shows the opposite pattern.
- *M, Nr, Rb* increase the Skin friction values whereas λ shows the opposite pattern.
- *M, Wi, n, Rd, Nt* declines Nusselt number values whereas *Pr* shows the opposite pattern.
- Motile microorganism density is boosted by increasing the *Lb* values and declining the *Pe* values.

7. Nomenclature

u, v	velocity components (m/s)
B_0	Magnetic field (A/m)
U_0	Velocity (m/s)
u_w	Stretching velocity (m/s)
α	First order slip velocity
β	Second order slip velocity
U_{slip}	Velocity slip (m/s)
Pr	Prandtl number
C_∞	Ambient fluid concentration (Mol/m^3)
λ	Mixed convection parameter
D_B	Browmian diffusion $(m^2 s^{-1})$
D_M	Microorganisms diffusion $(m^2 s^{-1})$
Nr	Buoyancy ratio
D_T	Thermophoresis diffusion
Nu_x	Local Nusselt number
σ	Electrical conductivity $\left(A^2 S^{-3}/\left(kg.m^2\right)\right)$
Lb	Bioconvection Lewis number
Sh_x	Sherwood number
Rd	Thermal radiation
Ec	Eckert number
Bi	Biot number
Rb	Bioconvection Rayleigh parameter
Nn_x	Microorganism Sherwood number
N_∞	Microorganism density $(kg.m^{-3})$
Le	Lewis number
T_∞	Temperature (Ambient fluid) (K)
Nt	Thermophoresis parameter
Nb	Browmian motion
Pe	Peclet number
ν	Kinematic viscosity (m^2/s)
Wi	Weissenberg number
n	Power law index
δ_1	Microorganism diffence parameter
σ^*	Chemical reaction (s^{-1})
W_c	Cell swimming speed (ms^{-1})
ρ	Density (kg/m^3)
T_w	Temperature at the surface (K)
C_w	concentration (Mol/m^3)
N	Microorganism density $(kg.m^{-3})$
N_w	Surface microorganism density $(kg.m^{-3})$

Orcid

Utpal Jyoti Das: 0000-0002-5482-5468
Nayan Mani Majumdar: 0000-0002-9590-068X

Declarations

Conflict of interest

The authors have no relevant financial or non-financial interests to disclose.

References

1. Ali A, Farooq H, Abbas Z, Bukhari Z, Fatima A. Impact of Lorentz force on the pulsatile flow of a non-Newtonian Casson fluid in a constricted channel using Darcy's law: a numerical study. Scientific reports. 2020 Jun 30;10(1):10629.

2. Alhadhrami A, Vishalakshi CS, Prasanna BM, Sreenivasa BR, Alzahrani HA, Gowda RP, Kumar RN. Numerical simulation of local

thermal non-equilibrium effects on the flow and heat transfer of non-Newtonian Casson fluid in a porous media. Case Studies in Thermal Engineering. 2021 Dec 1;28:101483.

3. Prameela M, Gangadhar K, Reddy GJ. MHD free convective non-Newtonian Casson fluid flow over an oscillating vertical plate. Partial Differential Equations in Applied Mathematics. 2022 Jun 1;5:100366.

4. Kumar MA, Reddy YD, Goud BS, Rao VS. An impact on non-Newtonian free convective MHD Casson fluid flow past a vertical porous plate in the existence of Soret, Dufour, and chemical reaction. International Journal of Ambient Energy. 2022 Dec 31;43(1):7410-8.

5. Eswaramoorthi S, Loganathan K, Faisal M, Botmart T, Shah NA. Analytical and numerical investigation of Darcy-Forchheimer flow of a nonlinear-radiative non-Newtonian fluid over a Riga plate with entropy optimization. Ain Shams Engineering Journal. 2023 Apr 1;14(3):101887.

6. Mirzaee H, Ahmadi G, Rafee R, Talebi F. Physical overview of the instability in laminar wall-bounded flows of viscoplastic and viscoelastic fluids at subcritical Reynolds numbers. Journal of Heat and Mass Transfer Research. 2023 Jun 1;10(1):135-46.

7. Das UJ, Majumdar NM, Shankar Goud B. Non-Darcian MHD flow of ternary-hybrid Cu-TiO2-Al2O3/H2O nanofluid over an inclined sheet with activation energy. Numerical Heat Transfer, Part B: Fundamentals. 2024 May 21:1-7.

8. Ibrahim W. Magnetohydrodynamics (MHD) flow of a tangent hyperbolic fluid with nanoparticles past a stretching sheet with second order slip and convective boundary condition. Results in physics. 2017 Jan 1;7:3723-31.

9. Khan M, Hussain A, Malik MY, Salahuddin T, Khan F. Boundary layer flow of MHD tangent hyperbolic nanofluid over a stretching sheet: a numerical investigation. Results in physics. 2017 Jan 1;7:2837-44.

10. Bibi M, Zeeshan A, Malik MY. Numerical analysis of unsteady momentum and heat flow of dusty tangent hyperbolic fluid in three dimensions. Scientific Reports. 2022 Sep 27;12(1):16079.

11. Salmi A, Madkhali HA, Nawaz M, Alharbi SO, Malik MY. Non-Fourier modeling and numerical simulations on heat and transfer in tangent hyperbolic nanofluid subjected to chemical reactions. International Communications in Heat and Mass Transfer. 2022 May 1;134:105996.

12. Faizan Ahmed M, Khalid M, Ali F, Al-Bossly A, Alduais FS, Eldin SM, Saeed A. Importance of bioconvection flow on tangent hyperbolic nanofluid with entropy minimization. Frontiers in Physics. 2023 Apr 7;11:1154478.

13. Gayatri M, Jayarami Reddy K, Jayachandra Babu M. Slip flow of Carreau fluid over a slendering stretching sheet with viscous dissipation and Joule heating. SN Applied Sciences. 2020 Mar;2:1-1.

14. Gopal D, Saleem S, Jagadha S, Ahmad F, Almatroud AO, Kishan N. Numerical analysis of higher order chemical reaction on electrically MHD nanofluid under influence of viscous dissipation. Alexandria Engineering Journal. 2021 Feb 1;60(1):1861-71.

15. Nalivela NR, Vempati SR, Ravindra Reddy B, Dharmendar Reddy Y. Viscous dissipation and thermal radiation impact on MHD mass transfer natural convective flow over a stretching sheet. Proceedings of the Institution of Mechanical Engineers, Part E: Journal of Process Mechanical Engineering. 2022 Mar 4:09544089221081339.

16. Li S, Khan MI, Alzahrani F, Eldin SM. Heat and mass transport analysis in radiative time dependent flow in the presence of Ohmic heating and chemical reaction, viscous dissipation: An entropy modeling. Case Studies in Thermal Engineering. 2023 Feb 1;42:102722.

17. Das UJ, Majumdar NM. An analytical study of magnetohydrodynamic Casson fluid flow in a channel with induced magnetic field, radiative heat flux and viscous dissipation. International Journal of Ambient Energy. 2023 Feb 25:1-7.

18. Das UJ, Majumdar NM, Patgiri I. Influence of thermophoretic deposition and viscous dissipation on magnetohydrodynamic flow with variable viscosity and thermal conductivity. Heat Transfer.

19. Ahmad S, Khan MN, Nadeem S, Rehman A, Ahmad H, Ali R. Impact of Joule heating and multiple slips on a Maxwell nanofluid flow past a slendering surface. Communications in Theoretical Physics. 2021 Dec 21;74(1):015001.

20. Waqas M, Sadiq MA, Bahaidarah HM. Gyrotactic bioconvection stratified flow of magnetized micropolar nanoliquid

configured by stretchable radiating surface with Joule heating and viscous dissipation. International Communications in Heat and Mass Transfer. 2022 Nov 1;138:106229.

21. Naseem T, Fatima U, Munir M, Shahzad A, Kausar N, Nisar KS, Saleel CA, Abbas M. Joule heating and viscous dissipation effects in hydromagnetized boundary layer flow with variable temperature. Case Studies in Thermal Engineering. 2022 Jul 1;35:102083.

22. Govindarajulu K, Reddy AS, Chamkha AJ. Entropy analysis on oscillating flow of third grade nanofluid in a channel with Joule heating: a Buongiorno model approach. The European Physical Journal Plus. 2023 May 17;138(5):416.

23. Sajid T, Sagheer M, Hussain S, Shahzad F. Impact of double-diffusive convection and motile gyrotactic microorganisms on magnetohydrodynamics bioconvection tangent hyperbolic nanofluid. Open Physics. 2020 May 2;18(1):74-88.

24. Shi QH, Hamid A, Khan MI, Kumar RN, Gowda RP, Prasannakumara BC, Shah NA, Khan SU, Chung JD. Numerical study of bio-convection flow of magneto-cross nanofluid containing gyrotactic microorganisms with activation energy. Scientific Reports. 2021 Aug 6;11(1):16030.

25. Waqas H, Khan SA, Alghamdi M, Alqarni MS, Muhammad T. Numerical simulation for bio-convection flow of magnetized non-Newtonian nanofluid due to stretching cylinder/plate with swimming motile microorganisms. The European Physical Journal Special Topics. 2021 Jul;230:1239-56.

26. Waqas H, Kafait A, Muhammad T, Farooq U. Numerical study for bio-convection flow of tangent hyperbolic nanofluid over a Riga plate with activation energy. Alexandria Engineering Journal. 2022 Feb 1;61(2):1803-14.

27. Shah SA, Ahammad NA, Ali B, Guedri K, Awan AU, Gamaoun F, Tag-ElDin EM. Significance of bio-convection, MHD, thermal radiation and activation energy across Prandtl nanofluid flow: A case of stretching cylinder. International Communications in Heat and Mass Transfer. 2022 Oct 1;137:106299.

28. Hussain S, Raizah Z, Aly AM. Thermal radiation impact on bioconvection flow of nano-enhanced phase change materials and oxytactic microorganisms inside a vertical wavy porous cavity. International Communications in Heat and Mass Transfer. 2022 Dec 1;139:106454.

29. Rashid U, Ullah N, Khalifa HA, Lu D. Bioconvection modified nanoliquid flow in crown cavity contained with the impact of gyrotactic microorganism. Case Studies in Thermal Engineering. 2023 Jul 1;47:103052.

30. Kaswan P, Kumar M, Kumari M. Analysis of a bioconvection flow of magnetocross nanofluid containing gyrotactic microorganisms with activation energy using an artificial neural network scheme. Results in Engineering. 2023 Mar 1;17:101015.

31. Aljaloud AS, Manai L, Tlili I. Bioconvection flow of Cross nanofluid due to cylinder with activation energy and second order slip features. Case Studies in Thermal Engineering. 2023 Feb 1;42:102767.

32. Wu L. A slip model for rarefied gas flows at arbitrary Knudsen number. Applied Physics Letters. 2008 Dec 22;93(25).